J Mater Sci (2012) 47:493–502
DOI 10.1007/s10853-011-5825-9

Gamma-ray irradiation induced structural and optical constants changes of thermally evaporated neutral red thin films

H. M. Zeyada · M. M. EL-Nahass · M. M. EL-Shabaan

Received: 30 May 2011 / Accepted: 26 July 2011 / Published online: 10 August 2011

Abstract Neutral red (NR) is polycrystalline in powder form, it transforms to nanocrystallite phase upon thermal deposition. Gamma-ray irradiation with doses 1.25–6 KGy induced partial transformation of nanocrystallite phase to amorphous structure. The changes of optical constants with γ-ray doses were calculated using spectrophotometer measurements of transmittance and reflectance at normal incidence of light over spectral range 200–2500 nm. The complex refractive index of NR film is highly influenced by exposure to γ-ray irradiation, the onset and optical energy gaps decrease with increasing γ-ray doses, and Urbach tail increases linearly with increasing irradiation dose. The type of electronic transition, oscillator, and electric dipole strengths and dispersion parameters were determined before and after irradiation. The spectral behavior of dielectric constant with γ-ray doses was also estimated.

Introduction

Organic semiconductors have many interesting physical properties and numerous technological applications. Azo compounds are a branch of organic semiconductors and have applications in light-induced photoisomerization process and reversible optical data storage [1, 2]. Phenazine is a family of azo compounds and the parent substance of many dye stuffs such as eurhodines, neutral red (NR), indulines, and safranines. NR, a subject of this study has many staining, biological, and industrial applications [3].

Application of NR in any of technological devices will certainly be provided as thin films. The processing parameters of thin films are: film thickness, annealing and substrate temperatures, and exposing films to irradiation [4].

The effects of irradiation on the electrical and photoelectrical properties of materials are of technological and scientific importance. Exposing materials to electromagnetic radiation or ionizing particles results in two effects. Transient effect caused by electron and hole generation and permanent effect causes changes in the lattice. Particle or γ-irradiation induces defects in the band gap which affects the free carrier concentration and leads to an increase and decrease in barrier height in *p*- and *n*-type semiconductors, respectively [5–7]. The irradiation-induced electrically active defects act either as traps or as recombination centers in the semiconductors, depending on capture cross-section of the electrons and holes [8].

Exposing organic semiconductors to light irradiation results in photo generated excitons (bound electron–hole pairs) that does not spontaneously dissociate into separate electron and hole; for carriers to be generated, excitons should be dissociated by means of external electric field or of specific dissociation sites or others. High energy radiation penetrates into metal–semiconductor interface and causes deep damage below the interface. Low energy radiation causes sever lattice damage in the form of vacancies, interstitials, defect complexes, and amorphization [9]. Gamma irradiation with energy >1 MeV induced coordination defects in As_2S_3-based chalcogenide semiconductor glasses [10]. These defects are created in the form of diamagnetic pairs of over and under coordinated

H. M. Zeyada (✉) · M. M. EL-Shabaan
Faculty of Science, Department of Physics, Mansoura University, Damietta Branch, New Damietta 34517, Egypt
e-mail: hzeyada@gmail.com

M. M. EL-Nahass
Faculty of Education, Department of Physics, Ain Shams University, Roxy, Cairo 11757, Egypt

atoms in the glass structure network with positive and negative electrical charge, respectively [11]. Gamma irradiation of the Ge-As(Sb)-S glasses lead to a long-wave shift of their fundamental absorption edge. This effect is supposed to be connected with bond rearrangements and atomic disorder changes [12]. Laser irradiation has been introduced in the fabrication of ZnO film with controlled defect density and desired smooth crystalline surface by adjusting laser energy density [13].

Depending on the sensitivity of the solid, the degree of disorder can range from point defects to a continuous amorphous zone along the ion path commonly called latent track. On the other hand, irradiation by low energy ionizing radiations like electrons produces a homogenous distribution of the absorbed dose. It has been observed that N-dangling bonds are generated by ion implantation in SiN_3 [14]. Moreover, ion irradiation has been employed for formation of amorphous [15] and polycrystalline Si_3N [16]. Upon high-energy ion irradiation, a gradual color change of unplasticized PVC copolymer films from colorless to dark brown is observed [17]. With increasing beam flux, both the optical energy gap and the width of the tail of localized states in the band gap changes. The concentration of the trapped radical species in the band gap depends on the irradiation flux.

In this study, we report on γ-ray irradiation induced structural and optical properties changes of thermally evaporated NR films.

Experimental details

A dark green powder of NR was used in this study. NR, 3-amino-7-(dimethylamino)-2-methyl-hydrochloride was purchased from Aldrich and was used in as-received condition without further purification. The molecular structure of NR is depicted in Fig. 1. Thin films of NR were sublimated by conventional thermal evaporation technique using high vacuum coating system (Edwards Co., Model E306A, England). The films were deposited onto clean glass substrates for X-ray diffraction (XRD) analysis and onto amorphous optical flat quartz substrates for optical measurements; the quartz substrates were carefully cleaned by immersing them in chromic acid for 15 min and then rinsed by deionized water. The material was sublimated from a quartz crucible source heated by a tungsten coil in a vacuum of 5×10^{-4} Pa. The rate of deposition was controlled at 2.5 nm/s by using a quartz crystal thickness monitor (Model, TM-350 MAXTEK, Inc. USA). The thickness was also monitored by using the same thickness monitor. A shutter fixed near to the substrate was used to avoid any probable contamination on the substrates in the initial stage of evaporation process and to control the thickness of films accurately. During deposition, the substrates were kept at room temperature ($\cong$300 K). After deposition, the film thickness was also checked interferometrically by Tolansky method [18].

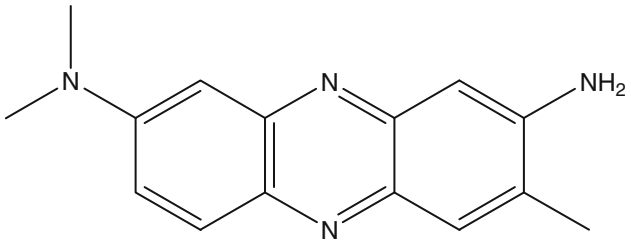

Fig. 1 Molecular structure of neutral red (NR)

XRD patterns of NR in powder form, as-deposited, and γ-ray-irradiated thin films were performed by XRD system (Philips X'pert MPD) equipped with Cu target. The Ni-filtered Cu K_α radiation ($\lambda = 1.5408$ Å) was used. The X-ray tube voltage and current were 40 kV and 30 mA, respectively.

The transmittance, $T(\lambda)$, and reflectance, $R(\lambda)$, spectra of the as deposited and gamma irradiated NR thin films with thickness 900 nm were measured at normal incidence of light in spectral range (200–2500 nm) using a double-beam spectrophotometer (JASCO model V-570 UV-Vis.-NIR). An uncertainty of 1% was given by the manufacturer for the measurements obtained by this spectrophotometer. A quartz blank substrate identical to the one used for thin film deposition was used as a reference for the transmittance scan. These measurements were also performed for the film after being exposed to different doses of γ-ray. The γ-ray doses were obtained from Technetium-99m generator (Bristol-Myers Squibb Pharma Belgium S.A.) and it ranges 1.25–6 KGy.

Calculation model

For a monochromatic beam of light impinging on a thin film deposited on a thick transparent substrate, multiple reflections occur at the interface of the system. Assuming that these reflections are coherent in thin films and incoherent in the substrate, the absolute expressions f or total measured transmittance, T, and reflectance, R, after introducing corrections resulting from absorption and reflection of the substrate are given by [19]:

$$T_{\exp} = \frac{I_{\mathrm{ft}}}{I_{\mathrm{q}}}\left(1 - R_{\mathrm{q}}\right), \tag{1}$$

where I_{ft} and I_{q} are the intensities of light passing through film-substrate system and reference, respectively. R_{q} is the reflectance at the substrate.

$$R_{\exp} = \frac{I_{\mathrm{fr}}}{I_{\mathrm{m}}} R_{\mathrm{m}} \left[\left(1 - R_{\mathrm{q}}\right)^2 + 1 \right] - T^2 R_{\mathrm{q}}, \tag{2}$$

where I_{fr} and I_{m} are the measured intensity of light reflected from the sample and aluminum reference mirror, respectively. R_{m} is the mirror reflectance.

The refractive index, n, the absorption coefficient, α, and the absorption index, k, can be calculated by using the following equations:

$$n = \left(\frac{4R}{(1-R)^2} - k^2 \right)^{1/2} + \left(\frac{1+R}{1-R} \right) \tag{3}$$

$$\alpha = \left(\frac{1}{d} \right) \ln \left[\left(\frac{(1-R)^2}{2T} \right) + \left(\left(\frac{(1-R)^4}{4T^2} \right) + R^2 \right)^{1/2} \right] \tag{4}$$

$$K = \frac{\alpha \lambda}{4\pi}. \tag{4a}$$

The errors in the calculated values of n and k were computed by a program comprising a modified bivariant search technique [20] based on minimizing $|\Delta T|^2$ and $|\Delta R|^2$ simultaneously, where

$$|\Delta T|^2 = \left| T_{(n,k)} - T_{\exp} \right|^2 \quad \text{and} \quad |\Delta R|^2 = \left| R_{(n,k)} - R_{\exp} \right|^2, \tag{5}$$

where $T_{(n,k)}$ and $R_{(n,k)}$ are the calculated values of transmittance and reflectance using Murmann's exact equations [21, 22]. $T_{\exp}$ and $R_{\exp}$ are the experimental absolute values measured from (1) and (2), respectively. By applying the technique adopted in [20], unique values of n and k are obtained within the desired accuracy. An optimization step-length technique follows to speed up the convergence as well as to shorten the run time needed to improve associated accuracy. The experimental errors are taken into account as follows: ±1% for T and R calculations, ±3% for refractive index, ±2.5% for absorption index, and ±2.5% for film thickness measurements.

Assuming that a solid has a density, ρ, and its molecular weight is M, the absorption coefficient can take the form [23]:

$$\alpha = 2303 \left(\frac{\rho}{M} \right) \xi_{\mathrm{molar}}(\nu_0) = G \xi_{\mathrm{molar}}(\nu_0), \tag{6}$$

where G is a constant that depends on the material. The oscillator strength, f, and the electric dipole strength, q^2, [24] can be deduced from spectral distribution of $\xi_{\mathrm{molar}}(\nu)$ using Gaussian fit and they are given as:

$$f = 4.32 \times 10^{-19} \int \xi_{\mathrm{molar}}(\nu_0) \mathrm{d}\nu_0 \tag{7}$$

$$q^2 = \frac{1}{2500} \xi_{\mathrm{molar}}(\nu_0) \frac{\Delta \lambda}{\lambda_0}, \tag{8}$$

where $\Delta\lambda$ is the width of wavelength for absorption at half intensity and λ_0 is the resonant wavelength.

The type of electron transition and value of optical energy gap, E_{g}, were determined from the analysis of α near the onset and the fundamental absorption edge using the equation introduced by Bardeen et al. [25] for amorphous semiconductors as:

$$\alpha h\nu = B(h\nu - E_{\mathrm{g}})^r, \tag{9}$$

where B is a constant related to electrical conductivity and energy level separation, $r = 2$ or 3 for indirect allowed and forbidden transitions, respectively, and $r = 1/2$ or 3/2 for direct allowed and forbidden transitions, respectively. Differentiating (9) with respect to $h\nu$ and dividing (9) by product of differentiation we obtain:

$$\left[\alpha h\nu \Big/ \left(\frac{\mathrm{d}(\alpha h\nu)}{\mathrm{d}(h\nu)} \right) \right] = \frac{1}{m} \left(h\nu - E_{\mathrm{g}} \right). \tag{10}$$

A plot of $\alpha h\nu \Big/ \frac{\mathrm{d}(\alpha h\nu)}{\mathrm{d}(h\nu)}$ versus $h\nu$ is a straight line. The reciprocal of the slope of the line determines the type of electronic transition, r, and extrapolation of straight line to intercept the abscissa is the energy gap, E_{g}.

The optical absorption below the absorption edge ($\alpha < 10^4$ cm^{-1}) can be analyzed by Urbach's role [26] as:

$$\alpha = \alpha_0 \exp \left(\frac{h\nu}{E_{\mathrm{u}}} \right), \tag{11}$$

where α_0 is a constant and E_{u} can be considered as the width of the tail of localized states in the forbidden band gap and it is an indicator to structural disorder of semiconductor.

In the transparent region of spectra, the spectral dependence of refractive index can be explained by adopting single oscillator model proposed by Wemple and Di Domenico [27], this model was applied for interpretation of results of covalent and ionic solids whether in amorphous or crystalline phase; they found that all optical data of refractive index in the transparent region can be described, to a good approximation, by the following relation [27]:

$$\frac{1}{n^2 - 1} = \frac{E_{\mathrm{o}}}{E_{\mathrm{d}}} - \frac{1}{E_{\mathrm{o}} E_{\mathrm{d}}} (h\nu)^2, \tag{12}$$

where $h\nu$ is the photon energy, E_{o} is the oscillator energy, and E_{d} is the oscillator strength or dispersion energy. The parameter E_{d} is a measure of the intensity of inter-band transition and it does not depend significantly on the band gap or the density of the valance electrons; however, E_{o} can be considered as an average value of the energy gap of the material.

The complex dielectric function, $\varepsilon*(\nu) = \varepsilon_1(\nu) + \mathrm{i}\varepsilon_2(\nu)$, describes the optical response of the medium at all

photon energies hv. The real, ε_1, and imaginary, ε_2, parts of dielectric constant were determined by the following relations [28]:

$$\varepsilon_1 = n^2 - k^2 = \varepsilon_L - \left(\frac{e^2}{4\pi^2 c^2 \varepsilon_0}\right)\left(\frac{N}{m^*}\right)\lambda^2 \quad (13)$$

$$\varepsilon_2 = 2nk = \frac{\varepsilon_\infty \omega_p^2}{8\pi^2 c^3 \tau}\lambda^3, \quad \omega_p = \left(\frac{e^2 N}{\varepsilon_0 \varepsilon_L m^*}\right)^{1/2}, \quad (14)$$

where ω_p is plasma frequency, ε_L is lattice dielectric constant, ε_∞ is the dielectric constant at infinite frequency, ε_0 is permittivity of free space, $\frac{N}{m^*}$ is ratio of carrier concentration to its effective mass, and τ is optical relaxation time.

Results and discussion

Structural analysis

Figure 2 shows the XRD pattern of NR in powder form, in as-deposited, and γ-ray-irradiated thin films. It is observed that the powder of NR is of polycrystalline structure, Fig. 2a, and it transformed to nanocrystallite phase upon thermal deposition, Fig. 2b. Identification of XRD pattern of NR in powder form by using Ref. [29] showed that it has triclinic crystal system and space group $p\bar{1}$ with lattice parameters: $a = 10.2675$ Å, $b = 14.773$ Å, $c = 16.454$ Å, $\alpha = 72.67°$, $\beta = 111.61°$, and $\gamma = 81.83°$. The indicated Miller indices (hkl) on each diffraction peak have been calculated by using CRYSFIRE system for automatic powder indexing and LMPG-Suite programs for the interpretation of X-ray experiments [29, 30]. For powder sample, a major peak is observed at about ($2\theta = 26°$) and its equivalent inter-planar spacing is 3.407 Å which corresponds to reflection from $(\bar{2}\bar{3}2)$ plane of triclinic crystal system.

For as-deposited film, a single peak is also observed around $2\theta = 24.935°$ as shown in Fig. 2b; this indicates that the nanocrystallites are preferentially oriented with $(1\bar{3}0)$ plane parallel to the surface of substrate. Upon exposing as-deposited film to γ-ray irradiation of doses 1.25 and 6 KGy, the $(1\bar{3}0)$ diffraction peak intensity of the sample was strongly reduced accompanied by narrowing of full width at half maximum (FWHM). This indicates decreasing of intrinsic structural defects in irradiated film. The peak position of $(1\bar{3}0)$ shifted from 24.935° for as-deposited film to 24.815° for γ-ray-irradiated film, which suggests increase of lattice constant upon irradiation and therefore decreasing its mass density. It is also observed that a hump is created in irradiated film in 20°–35° of 2θ range whose integrated intensity increases with irradiation dose. This shows that irradiated NR film is composed from a nanocrystallite and amorphous phases and the amorphization of the film increases with increasing irradiation dose. The increase of lattice parameter, narrowing of FWHM, and increasing of integrated intensity of the hump with the increase of irradiation dose are the characteristic structural features resulting from irradiation-induced partial amorphization. Irradiation-induced amorphization occurs when the free energy of the original crystalline phase is equal to or higher than that of its amorphous counterpart [31, 32]. Atomic displacements are suggested to be the reason for irradiation-induced amorphization [31]. The dynamic component of atomic displacement $\langle \mu_{vib}^2 \rangle$ scales directly with temperature and is a measure of free energy associated with phonons and static component of atomic displacement $\langle \mu_{sta}^2 \rangle$ is a measure of static atomic disorder stored in the lattice in the form of intrinsic and extrinsic lattice defects which gives rise to an increase in the free energy [33].

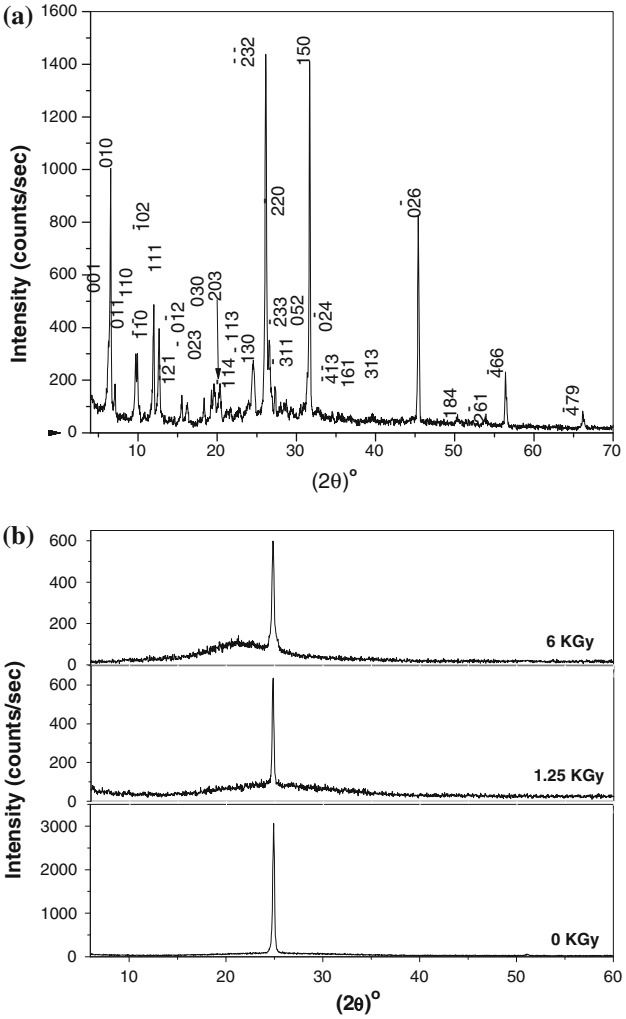

Fig. 2 **a** XRD pattern of NR in powder form and **b** XRD pattern of as-deposited and γ-ray-irradiated NR thin films

Optical properties

Spectral behavior of T(λ) and R(λ)

The spectral behavior of the transmittance, $T(\lambda)$, and the reflectance, $R(\lambda)$, at nearly normal incidence of light for as-deposited NR thin film of thickness 900 nm is presented in Fig. 3. This figure also contains results for the same film after being exposed to γ-ray irradiation of different doses (1.25, 2.5, 3.75, and 6 KGy). The transmission edge of as-deposited film divides the spectra into two regions: (a) in the wavelength range 200–680 nm; the total sum of $T(\lambda)$ and $R(\lambda)$ is less than unity (absorption region) and (b) at long wavelength, $\lambda > 680$ nm, the film becomes transparent and no light was absorbed, $T(\lambda) + R(\lambda) \approx 1$ (transparent region). There is a transmission band in absorption region in wavelength range 326–422 nm whose peak is at 373 nm. The results of T and R indicate that the film is homogeneous. Exposing film to γ-ray doses reduces the peak intensity of interference maxima and minima of transmittance and reflectance spectra and this reduction in intensity increases with increasing irradiation dose. No new transmission peaks are observed in all cases. It may be concluded that γ irradiation has no change on transmittance properties of films in absorption region of spectra. The width of transmission edge decreases with increasing irradiation doses, so we expect an influence of irradiation doses on energy gap and Urbach tail. In transparent region, the total sum of $T(\lambda)$ and $R(\lambda)$ is less than unity, indicating that there is an additional absorption which would be due to disorder in structure caused by γ-ray irradiation.

Absorption characteristics

Figure 4 represents spectral distribution of absorption index, k, for the as-deposited and γ-ray-irradiated NR thin film. There are two absorption bands in ultraviolet and visible region of spectra, which are attributed to electronic transitions between π and π^* orbital. There is also a sharp absorption edge in wavelength range 534–680 nm. At 680 nm, k starts to increase with increasing wavelength which is a characteristic feature of existence of free carriers. Exposing film to γ-ray irradiation decreases its absorption index and reduces peaks intensity in ultraviolet and visible region of spectra; this may be attributed to induced defect states in the band gap which increases with the increase in irradiation dose and it acts as trapping/recombination centers that reduces absorption. At $\lambda > 680$ nm, k increases with increasing irradiation dose for a fixed wavelength and it decreases with increasing wavelength for a fixed irradiation dose as it is illustrated in the inset of Fig. 4. Such a behavior indicates that an additional optical absorption is added to free carrier absorption existing in as-deposited thin film; we argue increasing of absorption index with increasing irradiation dose to increasing of disorder resulting from nanocrystallite to amorphous transformation.

The spectral behavior of molar extinction coefficient, $\xi(v_0)$, for as-deposited and γ-ray-irradiated NR film is illustrated in Fig. 5. The oscillator strength and electric dipole strength for as-deposited and γ-ray-irradiated NR film has been calculated using Gaussian fit and they are listed in Table 1. It is clear that γ-ray doses reduce values of oscillator and electric dipole strengths.

The type of optical transition and value of energy gap are illustrated in Figs. 6, 7. Figure 6 indicates that the type of electronic transition for as-deposited NR film is indirect allowed transition and onset energy gap is 1.75 eV. Figure 7a is a plot of $(\alpha hv)^{1/2}$ versus hv for as-deposited and γ-ray-irradiated NR film; irradiation doses do not change type of transition, as it is clear from inset of Fig. 7a an exponential decrease of onset energy gap with

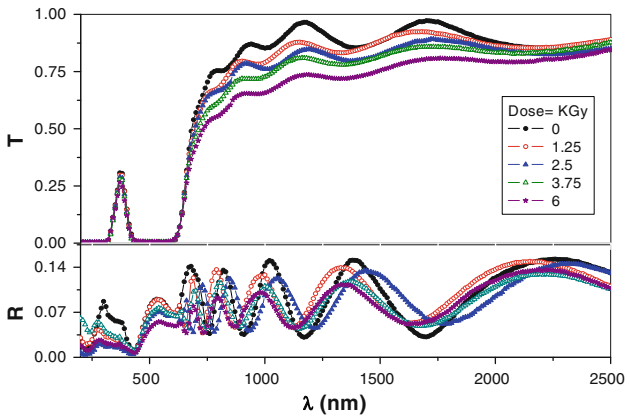

Fig. 3 Spectral behavior of transmittance, $T(\lambda)$, and reflectance, $R(\lambda)$, for as-deposited and γ-ray-irradiated NR thin films

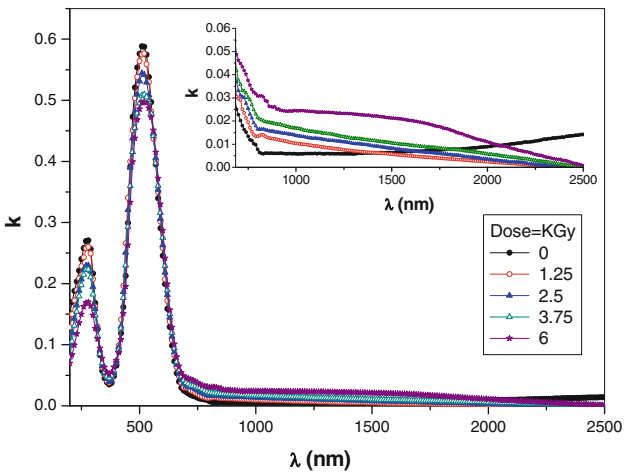

Fig. 4 Spectral behavior of absorption index, k, for the as-deposited and γ-ray-irradiated NR thin films

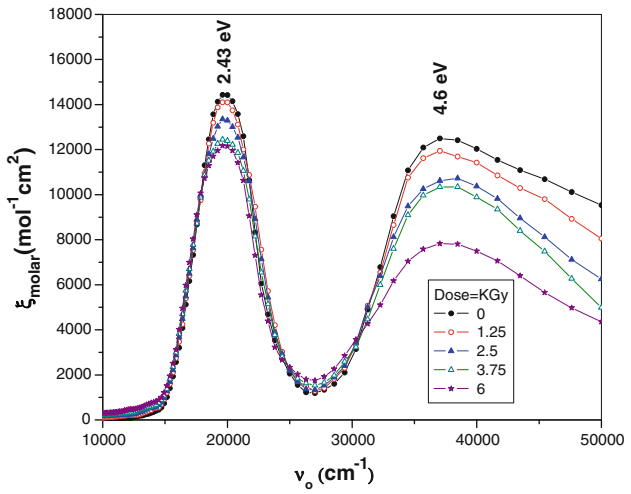

Fig. 5 Spectral behavior of molar extinction coefficient, $\xi_{molar}(\nu_0)$, for as-deposited and γ-ray-irradiated NR thin films

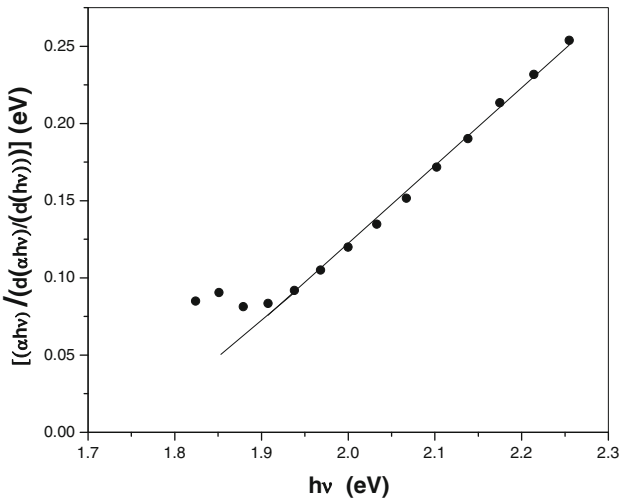

Fig. 6 Variation of $\left(\alpha h\nu \Big/ \frac{d(\alpha h\nu)}{d(h\nu)}\right)$ versus $h\nu$ for as-deposited NR film

increasing irradiation dose is observed, such a relation is controlled by an equation of the form:

$$E_{g,onset}^{ind} = 1.69 + 0.053\exp(-\text{dose}/4.32). \quad (15)$$

Figure 7b illustrates the variation of optical energy gap with γ-ray irradiation of different doses (1.25, 2.5, 3.75, and 6 KGy). A linear decrease in optical energy gap is observed with increasing irradiation dose and it obeys the formula:

$$E_{g,Opt}^{ind} = 3.24 - 0.05\text{dose}. \quad (16)$$

For optical absorption below the absorption edge ($\alpha < 10^4$ cm^{-1}), a plot of ln(α) versus $h\nu$ for as-deposited and irradiated NR thin film is illustrated in Fig. 8. A linear relationship is obtained verifying Urbach role (11). The reciprocal of the slope of each line is the magnitude of Urbach energy, E_u. A plot of Urbach's energy versus irradiation dose is shown in the inset of Fig. 8. E_u increases linearly with increasing radiation dose according to the relationship:

$$E_u = 181.66 + 28.35\text{dose}. \quad (17)$$

The increase of Urbach energy with irradiation dose indicates formation of defect states in the band gap.

The dependence of indirect allowed optical energy gap, E_g^{ind}, and the width of tail of localized states, E_u, on irradiation dose is collected and presented in Table 2. The decrease of optical energy gap with the increase in γ-ray irradiation dose has been reported in inorganic semiconductors [34, 35] as well as in organic semiconductors [36–38]. El-Sayed [34] showed that irradiation induced a decrease in energy gap of $SbSe_{2.5}$ film as the dose is increased. This behavior is believed to be associated with the generation of electronic localized states. The change in the optical gap may be explained in terms of defects in the structural bonding and crystal field mechanism [34]. Gamma irradiation of the Ge-As(Sb)-S glasses leads to a long-wave shift of their fundamental absorption edge [12]. This effect is supposed to be connected with bond rearrangements and atomic disorder changes [12]. Irradiation of TeO_2 thin films by different doses of γ-radiation resulted in a decrease of optical band gap with the increase in radiation dose [35]. The optical band gap of MnPc [37] and pyronine G(y) [38] films showed a decrease in their value with the increase in γ-rays radiation dose. El-Nahass et al. [36] reported that irradiation decreased the optical band gap and increased width of the tail of localized states in the forbidden gap of iron(III) chloride tetraphenylporphyrine.

Table 1 Values of oscillator and electric dipole strengths for as-deposited and γ-ray-irradiated NR thin film

Value of dose (KGy)	f		q^2 (Å)^2	
	Peak position at $E = 2.43$ (eV)	Peak position at $E = 4.6$ (eV)	Peak position at $E = 2.43$ (eV)	Peak position at $E = 4.6$ (eV)
0	0.365	0.65	1.28	1.23
1.25	0.364	0.63	1.326	1.19
2.5	0.351	0.602	1.271	1.21
3.75	0.34	0.59	1.22	1.1
6	0.32	0.57	1.17	1.07

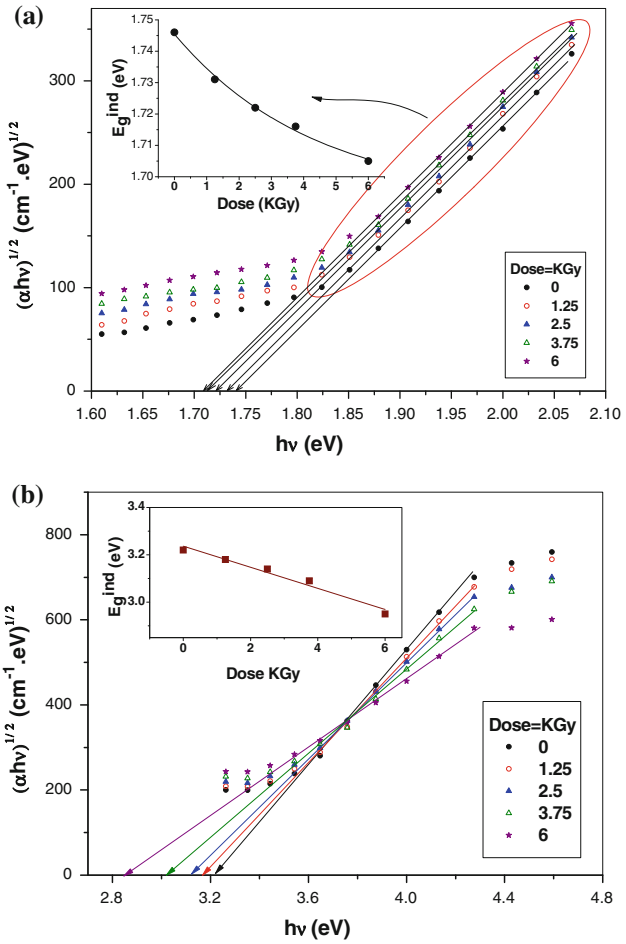

Fig. 7 **a** Variation of $(\alpha h\nu)^{1/2}$ versus $h\nu$ for onset absorption edge of as-deposited and γ-ray-irradiated NR thin films and **b** variation of $(\alpha h\nu)^{1/2}$ versus $h\nu$ for the optical absorption edge for as-deposited and γ-ray-irradiated NR thin films

Table 2 Indirect allowed energy gap and the width of Urbach tail for as-deposited and γ-ray-irradiated NR thin film

Dose (KGy)	$E_{g,onset}^{ind}$ (eV)	$E_{g,opt}^{ind}$ (eV)	E_u (meV)
0	1.746	3.22	186
1.25	1.731	3.18	211
2.5	1.722	3.14	245
3.75	1.716	3.09	301
6	1.705	2.95	348

In this study, the decrease of onset and optical energy gaps with increasing irradiation dose is believed to be a result of atomic disorder associated with nanocrystalline to partial amorphous transformation; this result in formation of defect states in the band gap which increases with the increase in irradiation dose as indicated by the increase of Urbach energy.

Dispersion characteristics

The spectral distribution of refractive index, n, for films in as-deposited condition and that for those after being exposed to γ-rays irradiation is illustrated in Fig. 9; it shows three bands and a shoulder in the ultraviolet and visible region of spectra which can be explained by adopting multioscillator model. At wavelength >680 nm, the spectral behavior of n is normal dispersion at which single oscillator model is applicable; in this region of spectra, we can deduce dielectric functions and oscillation parameters at high frequencies. Exposing film to γ-ray irradiation decreases its refractive index and reduces peak intensity present in ultraviolet and visible region of spectra. The relationship between refractive index and irradiation dose at constant wavelength of 1200 nm is shown in the inset of Fig. 9; a linear decrease of refractive index with

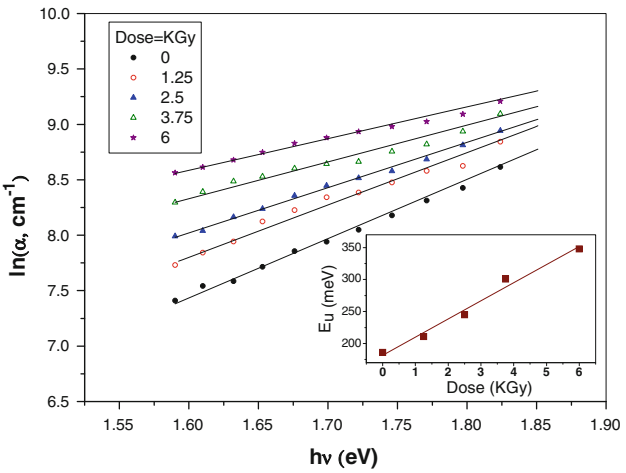

Fig. 8 Relation between ln(α) versus $h\nu$ for the as-deposited and γ-ray-irradiated NR thin films

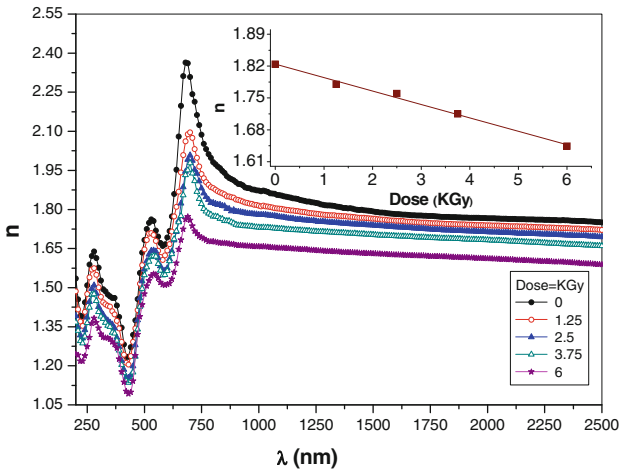

Fig. 9 Spectral behavior of refractive index, n, for the as-deposited and γ-ray-irradiated NR thin films

increasing irradiation dose is observed and it obeys the relation:

$$n = 1.824 - 0.0295\text{dose}. \quad (18)$$

The decrease of refractive index with increasing irradiation dose is correlated with a decrease of mass density [39]. The decrease of mass density of NR film is a result of increase of lattice parameter of NR as shown from XRD analysis.

A plot of $(n^2-1)^{-1}$ versus $(h\nu)^2$ for films in as-deposited condition and for those after being exposed to γ-ray irradiation is illustrated in Fig. 10. E_o and E_d are directly determined from the slope $(E_oE_d)^{-1}$ of the linear portion of the curve and its intercept with ordinate (E_o/E_d). The variation of E_o and E_d versus irradiation dose is shown in the inset of Fig. 10. The oscillator energy E_o and dispersion energy E_d have been reported to be related to the bond length L in the way $E_o \propto L^{-s}$ [40] and E_d depends on L^s [41], with s varying in the range $2 < s < 3$ [40]. The variation of E_o and E_d with irradiation dose may be interpreted on the basis that γ-ray irradiation induced partial transformation of nanocrystallite phase of NR into amorphous structure and this requires displacing host atoms and rearranging of the bonds which results in influencing bond length with a degree depending on irradiation dose. The values of high frequency dielectric constant, ε_∞, were determined by extrapolating straight portion of each curve to intersect with ordinate.

The spectral distribution of real dielectric constant, ε_1, versus λ^2 is depicted in Fig. 11; ε_1 decreases with increasing irradiation dose and square of wavelength. The decrease of ε_1 with the increase of irradiation dose is consistent with the decrease of the ratio of free carrier concentration to its effective mass as shown in Fig. 12. At long wavelength, the dependence of ε_1 on λ^2 is linear. The values of lattice dielectric constant, ε_L, were

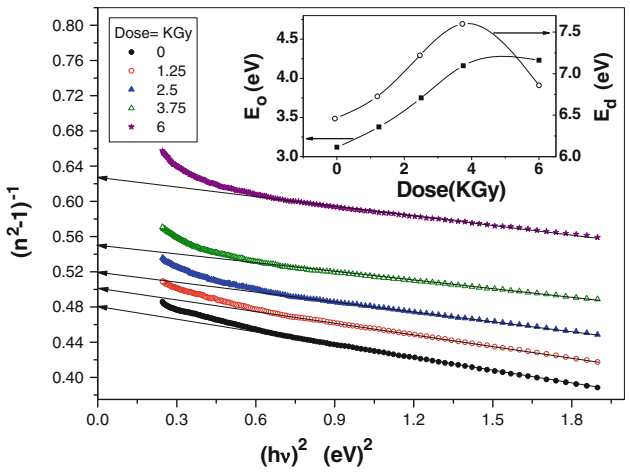

Fig. 10 Dependence of $(n^2-1)^{-1}$ on $(h\nu)^2$ for the as-deposited and γ-ray-irradiated NR thin films

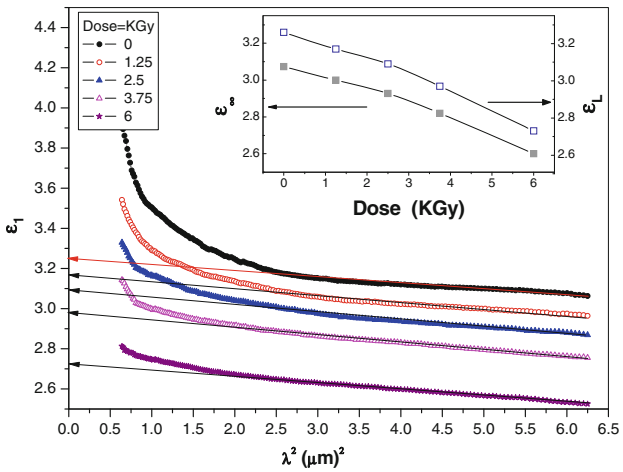

Fig. 11 Dependence of real part of the dielectric constant, ε_1, on λ^2 for the as-deposited and γ-ray-irradiated NR thin films

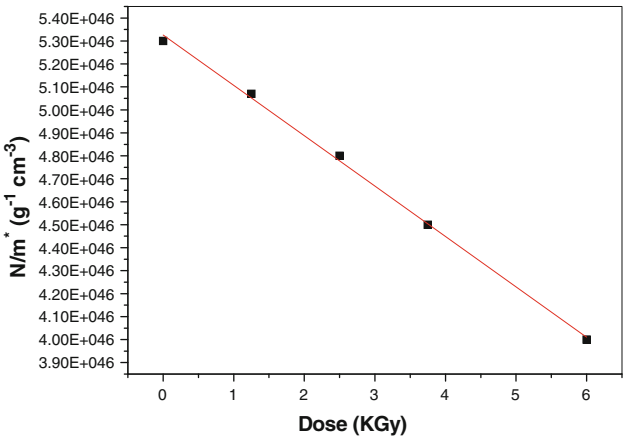

Fig. 12 N/m^* versus radiation dose for NR thin films

determined by extrapolating straight portion of each curve to intersect with ordinate. The variation of ε_L and ε_∞ versus radiation dose is illustrated in the inset of Fig. 11; a linear decrease of ε_L and ε_∞ with increasing irradiation dose is observed. It is noticed that the value of ε_L is $>\varepsilon_\infty$ and this may be attributed to free carrier absorption.

The ratio of carrier concentration to its effective mass versus irradiation dose is depicted in Fig. 12. A linear decrease of N/m^* with increasing irradiation dose is observed; such a trend follows an equation of the form:

$$\frac{N}{m^*} = 5.3 \times 10^{46} - 2.19 \times 10^{45}\text{dose}. \quad (19)$$

Dielectric characteristics

Figure 13 is a spectral distribution of ε_1 for as-deposited and γ-ray-irradiated NR thin film, it shows peaks at 1.8, 2.3, and 4.44 eV and a shoulder in energy range (3.36 → 3.88 eV). The general trend is the decrease of ε_1

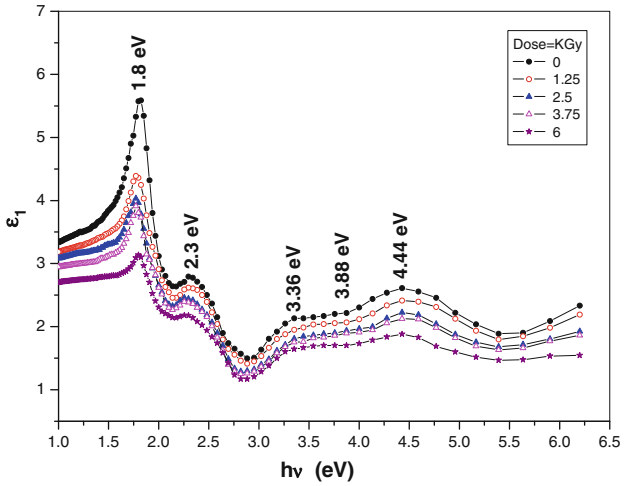

Fig. 13 Spectral behavior of ε_1 for as-deposited and γ-ray-irradiated NR thin films

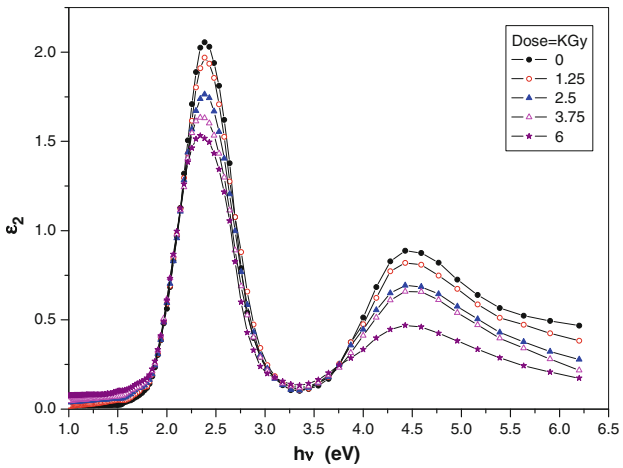

Fig. 14 Spectral behavior of ε_2 for as-deposited and γ-ray-irradiated NR thin films

with increasing frequency. The polarization processes influencing dielectric constant of a material are: ionic, electronic, dipolar, and interfacial or surface polarization. The spectral behavior of dielectric constant determines type of operating polarization process. In crystalline and nanocrystalline materials, grain boundaries are considered as preferable sites for accumulation of defects, such as dangling bonds, vacancies, ions, etc. Associated with such defects, a space charge distribution which can move under the application of external field and then trapped by defects resulting in space charge polarization, ion jump polarization may also be greater in nanocrystalline materials. In this study, the large value of dielectric constant at low frequency is due to the presence of space charge dominated at low frequency as shown in Fig. 4. When the frequency is increased, the dipoles of polarized space charge will no longer be able to rotate sufficiently rapidly, so their oscillation will begin to lay behind the field, which explains the observed decrease in ε_1 with frequency. Nanocrystallite to amorphous solid state transformation decreases lattice defects [32]. Therefore, dielectric constant decreases with increasing γ-ray irradiation doses.

Figure 14 is a spectral distribution of ε_2 for as-deposited and γ-ray-irradiated NR thin film. ε_2 increases with increasing energy and it has a sharp absorption edge at 1.746 eV and an absorption band starting at about 3.5 eV. ε_2 has absorption peaks at 2.37 and 4.43 eV whose peaks decreases with increasing irradiation dose. The plasma frequency dependence on irradiation dose was calculated and is illustrated in Table 3. Plasma frequency decreases with increasing irradiation dose; this is attributed to the decrease of N/m^* with increasing irradiation dose.

Conclusions

NR is polycrystalline in as-synthesized condition, it transforms to nanocrystallite phase upon thermal deposition. Gamma-ray irradiation induced partial amorphization of nanocrystallite phase. The volume of amorphous phase depends on γ-ray irradiation dose.

Different doses of γ-ray could not change the transmittance and reflectance properties of NR film. The spectral behavior of absorption index showed band to band transition in wavelength range 200–680 nm and free carriers absorption at wavelengths >680 nm. Gamma-ray irradiation doses introduced additional absorption to free carrier absorption. Free carrier absorption is predominant at wavelength >2080 nm for as-deposited film. The oscillator and electric dipole strengths decrease with increasing γ-ray irradiation doses. The type of electronic transition for as-deposited and γ-ray-irradiated NR film is indirect allowed transition. The onset and optical energy gaps for as-deposited film is 1.75 and 3.23 eV, respectively. An exponential decrease of onset energy gap with increasing irradiation dose is observed. The optical energy gap decreases linearly with increasing irradiation dose. The refractive index decreases linearly with increasing irradiation dose. The variation in refractive index with γ-ray irradiation doses facilitates the possibility of applying NR in γ-irradiation dosimeter, planar waveguides as well as in nonlinear optics applications. The oscillator and dispersion energies decrease linearly with increasing γ-ray irradiation doses. The spectral behavior of ε_1 indicates that space charge polarization is predominant at low frequencies.

Table 3 Dispersion parameters of as-deposited and γ-ray-irradiated NR thin film

Dose (KGy)	ε_∞	ε_L	E_o (eV)	E_d (eV)	N/m^* (10^{45} g^1 cm^{-3})	ω_p (10^{14}/s)
0	3.073	3.26	3.12	6.46	53	2.17
1.25	3	3.17	3.38	6.728	51	2.15
2.5	2.927	3.09	3.75	7.22	48	2.11
3.75	2.82	2.97	4.16	7.6	45	2.09
6	2.6	2.73	4.23	6.86	40	2.05

References

1. Biswas N, Umapathy S (1997) J Phys Chem A 101:5555
2. Ayden ME, Türüt A (2007) Microelectron Eng 84:2875
3. Sabnis RW (2010) Handbook of biological dyes and stains. Synthesis and industrial application. John Wiley & Sons, Inc.
4. El-Nahass MM, Zeyada HM, Hendi AA (2000) Opt Mater 25:43
5. Manour H, Sellai A, Bouziane k, Al Harthy SH, Al Busidi M, Gard FS (2007) Vacuum 57:51
6. Fonash SJ, Ashok S, Singh R (1981) Appl Phys Lett 39:423
7. Grussell E, Berg S, Anderson LP (1980) J Electrochem Soc 127:573
8. Jayavel P, Udhayasankar M, Kumar J, Asokan K, Kanjilal D (1999) Nucl Instrum Methods B 156:110
9. Aliyu YH, Morgen DV, Bunce RW (1993) Phys Status Solidi (a) 135:119
10. Shpotyuk OI (1994) Phys Status Solidi (a) 145:69
11. Fritzsche H (1993) Philos Mag B 68:561
12. Shpotyuk OI, Golovchak RYa, Kavetsky TS, Kovalskiy AP, Vakiv MM (2000) Nucl Instrum Methods B 166–167:517
13. Zahao Y, Jiang Y (2010) Spectrochim Acta Part A 76:336
14. Paloura EC, Mertens A, Saitoh K, Ikeyama M, Holdack H (1996) Nucl Instrum Methods B 113:23
15. Miyagawa S, Nakao S, Saitoh K, Ikeyama M, Niwa H, Tanemura S, Miyagawa Y, Baba K (1995) J Appl Phys 78:7018
16. Li ZL, Leung JW, Deenapanary PNK, Conway M, Chivers DJ, Gerald JDF, Williams JS (1999) Nucl Instrum Methods B 148:534
17. Abdel-Fattah AA, Abdel-Hamid HM, Radwan RM (2002) Nucl Instrum Methods B 196:279
18. Tolansky S (1970) Multiple-beam interference microscopy of metals. Academic Press, London
19. Agiev LA, Shklyarevskii IN (1978) J Prekl Spekt 76:380
20. Soliman HS, El-Kadry N, Gamjoum O, El-Nahass MM, Darwish HB (1988) Indian J Opt 17(2):46
21. Heavens OS (1964) In: Hass G, Thus R (eds) Physics of thin films. Academic Press, New York
22. Liddeli HM (1981) Computer-aided technique for the design of multilayer filters. Hilger, Bristol
23. Schechtman BH, Spicer WE (1970) J Mol Spectrosc 33:28
24. Kumar GA, Thomas J, George N, Kumar BA, Radhakrishnan P, Nampoori VPN, Vallabhan CPG (2000) Phys Chem Glasses 41(2):89
25. Bardeen J, Blatt FJ, Hall LH (1956) In: Breckenridge R, Russel B, Hahn T (eds) Proceedings of photo conductivity conference. Wiley, New York
26. Urbach F (1953) Phys Rev 92:1324
27. Wemple SH, Di Domenico H (1971) Phys Rev B 3(4):1338
28. Edward PO (1985) Hand book of optical constants of solids. Academic Press, New York
29. Shirley R (2000) The CRYSFIRE system for automatic powder indexing: user's manual. The Lattice Press, Guildford
30. Laugier, Bochu B (2000) ENSP/Laboratoire des Materiaux et du Genie Physique. Saint Martin d'Heres
31. Motta AT (1997) J Nucl Mater 244:227
32. Beke DL, Bakker H, Loeff PI (1991) Acta Metall Mater 39:1259
33. Lam NQ, Okamoto PR, Li M (1997) J Nucl Mater 251:89
34. El-Sayed SM (2004) Nucl Instrum Methods Phys Res B 225:535
35. Arshak K, Korostynska O (2002) Sensors 2:347
36. El-Nahass MM, El-Deeb AF, Metwally HS, Hassanien AM (2010) Solid State Sci 12:552
37. Arshak A, Zleetni S, Arshak K (2002) Sensors 2:174
38. Soliman HS, El-Barry AMA, Yaghmour S, Al-Solami TS (2009) J Alloys Compd 481:390
39. Andreas B, Breunig I, Buse K (2005) Chem Phys Chem 6:1
40. Chen H, Shen WZ (2005) Eur Phys J B 43:503
41. González-Leal JM, Ángel JA, Márquez E, Jiménez-Garay R (2007) J Phys Chem Solids 68:987